Elastic Waves in Curved Space: Mimicking a Wormhole

Jian Zhu,[1,2,†] Yongquan Liu,[2,†] Zixian Liang,[3] Tianning Chen,[1] and Jensen Li[2,4,*]
[1]School of Mechanical Engineering and State Key Laboratory of Strength & Vibration of Mechanical Structures, Xi'an Jiaotong University, Xi'an, Shaanxi 710049, China
[2]School of Physics and Astronomy, University of Birmingham, Birmingham B15 2TT, United Kingdom
[3]College of Electronic Science and Technology, Shenzhen University, Shenzhen 518060, China
[4]Department of Physics, The Hong Kong University of Science and Technology, Clear Water Bay, Kowloon, Hong Kong, China

(Received 27 April 2018; published 5 December 2018)

Transformation optics (TO) can be used to investigate nontrivial spacetime structures with inhomogeneous materials. However, the extreme curvature and large refractive indices make the implementation of a wormhole challenging. By considering flexural waves on a curved plate with geometric curvature, the stringent material requirement can be relaxed, and we demonstrate a two-dimensional analog of a wormhole using homogeneous materials within a curved laboratory frame. TO is used to understand wave propagation in such a curved space. This curved elastic space approach allows us to investigate not only geodesics but also wave redirection, tunneling, and virtual caustics of the wormhole, and will be useful to develop curvature-driven wave front shaping in general.

DOI: 10.1103/PhysRevLett.121.234301

Transformation optics (TO) [1,2] provides a powerful tool to design nontrivial optical devices with inhomogeneous optical media, such as invisibility cloaks [3–5], illusion devices [6,7], and omnidirectional concentrators [8,9]. The same framework was used to construct specific lenses, such as the Maxwell fisheye and Luneburg lenses on an on-chip environment [10–12]. However, TO devices with extreme functions require extreme values of refractive indices. To ease fabrication and design, one can seek an optimal coordinate transformation [13,14]. One can also use the geometric curvature of the sample to get a smaller range of required indices [15]. The latter approach has an origin from general relativity, in which geometric curvature can be interpreted as mass being equivalent to the refractive index in wave propagation [16,17]. Conversely, it allows TO media to mimic some of the analog effects of cosmological objects with curved metrics such as an artificial black hole and a cosmic string in a laboratory environment [18–22]. On the other hand, one can use tunable materials, e.g., a space-time cloak [23] if we would like to implement the temporal effect of curved space-time, or use hyperbolic metamaterial with one spatial direction to emulate time [24].

In 2007, Greenleaf *et al.* [25] proposed a TO medium to mimic a wormhole which allows light travels through an invisible tunnel [26,27]. Its analog in plasmonics was then proposed [28]. Although light does not travel instantaneously between two distant points in the case of an actual wormhole, the proposed TO recipe provides a valuable platform to visualize some of the interesting consequences of the curved metrics predicted for cosmological objects. However, the required extremely anisotropic TO medium makes its experimental realization a challenge so far. In this Letter, we propose to use a homogeneous sample with pure geometric curvature to obtain the required TO medium. We experimentally mimic an embedded version of a wormhole using flexural waves propagating on a curved plate. We show that an effective refractive index profile, even with an infinite value, can be achieved merely by geometric curvature. Compared with existing approaches in studying geodesics in curved spaces [29–31], we can also investigate wave propagation in curved space by adopting a TO-based framework, allowing us to investigate lensing and wave tunneling through the elastic analog wormhole. We can also apply geometric curvature to other TO applications in the future, e.g., to control local field enhancement [32], optical gradient forces [33], waveguiding [34], on-body communication [35], and acoustic surface wave sensing [36,37].

The space-time metric of a traversable wormhole is hyperbolic in nature. By considering the metric at constant time and polar angle, it becomes a spacelike two-dimensional surface, and it is possible for it to be embedded in three-dimensional Euclidean space. It is called the embedding diagram of a wormhole [38] [Fig. 1(a)]. The top and bottom surfaces representing two different "universes" are linked adiabatically by a hollow tunnel. The tunnel is rotationally symmetric and has a radius a at its throat at $z = 0$. The spatial curvature of the wormhole is described by its metric $ds^2 = d\rho^2 + dz^2 + \rho^2 d\phi^2$, where s is the distance between two neighboring points in cylindrical coordinates (ρ, ϕ, z) in Euclidean space. We also denote r as the proper radial distance from the throat of the tunnel. It has a positive (negative) value on the top (bottom) surface. The shape of the embedded surface can be specified by a relationship

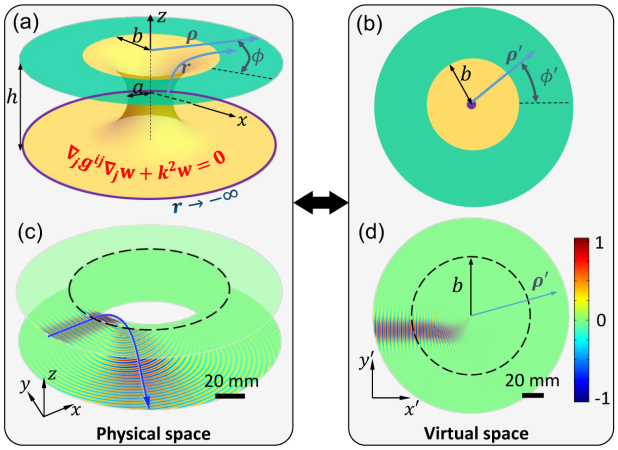

FIG. 1. Embedding diagram for the wormhole and transformation equivalence. (a) Schematic of the wormhole at a constant time in physical space. (b) The wormhole is transformed to a flat plane in virtual space for numerical simulation, the top surface with $\rho \geq b$ is mapped into $\rho' \geq b$ (green), and the tunnel and the bottom surface are compressed into $0 < \rho' \leq b$ (yellow). (c), (d) A Gaussian beam tunnels from the top to bottom surface. The scalar wave equation ($\nabla_i g^{ij} \nabla_j w + k^2 w = 0$) is transformed to virtual space and numerically solved. The same scalar field w is plotted in both spaces, with $b = 54.5$mm, $a = 34.5$mm, $h = 40.0$ mm.

between z and ρ. Without losing generality, we consider an elliptical shape for the tunnel:$[(b-\rho)/(b-a)]^2 + (2z/h)^2 = 1$, where b termed as the radius of the wormhole defines a boundary whose space is completely flat outside. h is the distance between the two flat surfaces with $\rho > b$.

In this work, we consider scalar wave propagation [of the field $w(r, \phi)$] around the wormhole, satisfying a Helmholtz equation $\nabla_i g^{ij} \nabla_i w + k^2 w = 0$ with $g_{rr} = 1$, $g_{\phi\phi} = \rho^2$, and $g_{r\phi} = 0$. TO is used to solve the scalar wave propagation in 2D curved space. The wormhole being embedded in Euclidean space [Fig. 1(a), termed the physical space] is further transformed to a flat 2D plane in Fig. 1(b) termed the virtual space. The mapping is chosen as $\rho' = be^{(r-r_b)/b}$ (for $-\infty < r < r_b$) and $\rho' = r - r_b + b = \rho$ (for $r \geq r_b$), where r_b is the proper radial distance from the throat to the location $\rho = b$ on the top surface. For both regions, $\phi' = \phi$ is used. The top surface with $\rho \geq b$ is thus mapped into $\rho' \geq b$ (green), and the tunnel and the bottom surface are compressed into the circular disk $\rho' \leq b$ (yellow). The infinite boundary of the bottom surface $r \to -\infty$ is now mapped to the origin $\rho' = 0$. As $r \in (-\infty, \infty)$ is mapped to $\rho' \in (0, \infty)$, the transformed Helmholtz equation is numerically solved in virtual space using a standard full-wave simulation package (COMSOL Multiphysics, 2D PDE module) with a set of transformed metric coefficients g'_{ij}, with details listed in the Supplemental Material [39].

To physically implement the embedding diagram of the wormhole with scalar wave propagation, we turn the curved surface in Fig. 1(a) into a curved thin plate of the same shape but a finite thickness d_0 and consider a flexural wave with wavelength λ propagating on it. The flexural wave here is described by the thin shell equation in the limit of small curvature (locally flat with $k^4 h^2 d_0^2 \gg 1$) $\nabla^2 D \nabla^2 w + \rho d_0 (\partial^2 w/\partial t^2) = 0$, where w is the out-of-plane displacement, ρ is the density, D is the bending stiffness, and $\nabla^2 = \nabla_i g^{ij} \nabla_j$ is the Laplace operator [30,40]. The wave equation (with time dependence $e^{-i\omega t}$) can be factorized into

$$(\nabla^2 + k^2)(\nabla^2 - k^2) w = 0, \tag{1}$$

where $k = \sqrt[4]{\omega^2 \rho d_0 / D}$. By considering propagating waves only, it can be approximated as the Helmholtz equation $(\nabla^2 + k^2) w = 0$ of the embedded wormhole [41,42]. It is interesting to note that the flexural wave equation with an inhomogeneous medium was used to construct elastic wave cloaks by the transformation approach [43–45].

As the first example to show the wave propagation around the wormhole, we investigate the situation and the condition for a beam to tunnel through the wormhole. The geometric parameters of the wormhole structure, to be experimentally realized later, are chosen to have radius $b = 54.5$ mm, tunnel radius $a = 34.5$ mm, and separation between the two "universes" as $h = 40$ mm. A Gaussian beam with wavelength $\lambda = 3.45$ mm and beam waist 4λ is incident along the positive x direction with an offset of 4λ in the y direction on the top surface. The scalar field distribution (w) obtained from the TO is equivalently shown in Figs. 1(c) and 1(d) in physical or virtual space. The beam tunnels to the bottom surface and changes direction (with some diffraction) through the curvature of the wormhole [Fig. 1(c)]. On the other hand, its equivalent field in virtual space [TO medium in Fig. 1(d)] has the beam converging towards the origin, since the mapping folds the infinite boundary of the bottom surface to the origin in virtual space. In this regard, we have implemented a TO device with refractive index [39] approaching infinity at the origin ($\rho' = 0$) for an observer on the flat top surface in physical space. The scalar field in Fig. 1(c) is also verified by 3D full-wave simulation for flexural waves on an elastic curved plate where the out-of-plane displacement satisfies approximately the Helmholtz equation (see Ref. [39] for the 3D simulation details).

Ray tracing is further conducted on the wormhole structure. The obtained ray trajectory is indicated by the blue arrow in Fig. 1(c) and is "scattered" through an angle of 118° from its original direction when it tunnels to the bottom surface, agreeing well with the scalar wave simulation (through a TO framework). A series of horizontal rays with different offset y_0 in the y direction is then performed with the ray trajectories shown in Fig. 2. When the offset $|y_0| \geq b$, the ray stays on the top flat space and travels in a straight line. When $a \leq |y_0| \leq b$, the ray is scattered by the curvature of the top surface but stays on the top surface all the time, represented by the typical ray in

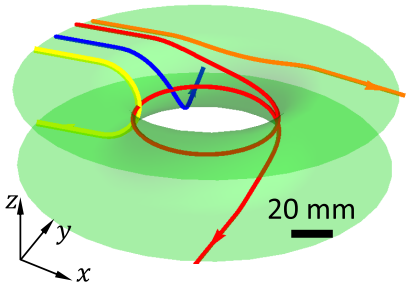

FIG. 2. Ray trajectories of horizontal rays with different incident positions on the top surface with the same dimensions as in Fig. 1(c).

orange. When $|y_0| \leq a$, the ray tunnels to the bottom surface [yellow (blue) ray for $y_0 = 0/0.5a$ with scattered angle 180°(100°)]. a is actually the radius of no return expected by the consideration of angular momentum (see Supplemental Material [39] for the ray-tracing method and point of no return). When $|y_0|$ approaches a from a smaller value, ray tracing predicts that the ray can go around the tunnel several times (the red ray) with an exit angle on the bottom surface being very sensitive to y_0. In fact, the ray picture breaks down in this case for a finite wavelength. The beam stays partially on the top surface and partially tunnels to the bottom surface with a dispersed field pattern rather than a well-defined beam, which is confirmed in full-wave simulations [39].

The tunneling phenomenon considered for a beam is a generic feature of wave propagation around the wormhole, which is actually not limited to rays only. Suppose the wormhole structure interacts with a vortex wave of angular momentum l. As the wormhole is rotationally symmetric, it preserves the angular momentum, and we would like to investigate whether tunneling still occurs. In this case, the waves change more abruptly than a Gaussian beam, and perfect tunneling may not occur. Mode conversion can occur for an elastic curved plate implementation. In the following, we show directly the flexural wave simulation for the 3D elastic curved plate. An inward traveling flexural vortex wave is excited by a force distribution at the outer boundary of the top plate with profile $\exp(il\phi)$ along ϕ and being homogeneous along z. The out-of-plane displacement at the middle plane of the plate obtained from simulation at wavelength $\lambda = 26.7$ mm and $l = 0$ is shown in Fig. 3(a). An outward propagating monopolar radiation pattern with the same amplitude is observed on the bottom plate, indicating that tunneling occurs. The same effect is also observed for different angular momenta up to $l = 6$. Figure 3(c) shows the example of $l = 3$ incidence towards the center, where a vortex with the same angular momentum appears at the bottom plate also with the same amplitude.

To quantify the tunneling effect, we calculate the tunneling efficiency for the flexural mode. For an incident flexural wave with angular momentum l, it has out-of-plane displacement $w_{\text{in}} = s_{\text{in}} H_l^{(2)}(k\rho)e^{il\phi}$ outside the tunnel on

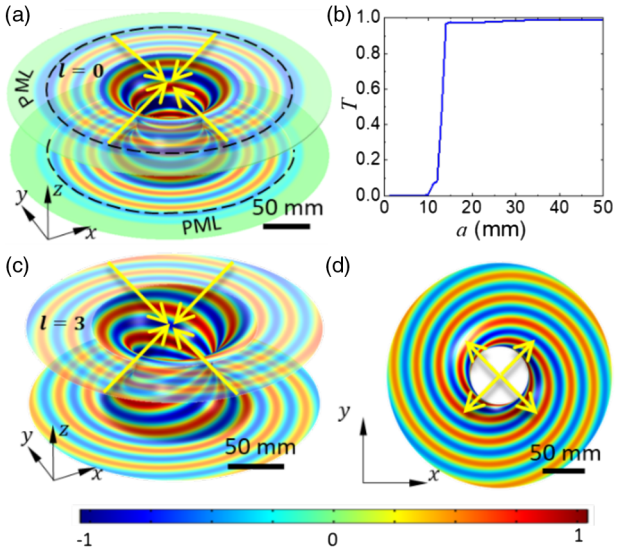

FIG. 3. Tunneling of vortex waves through the wormhole for its elastic plate implementation (with $a = 35$ mm, $b = 75$ mm, $h = 80$ mm, $d_0 = 2$ mm). (a) Simulated out-of-plane displacement of the middle plane of the plate for $l = 0$. (b) Tunneling efficiency T against a for $l = 3$. (c),(d) Out-of-plane displacement field for $l = 3$ on the whole structure and on the bottom plate. A perfectly matched layer (PML) is used at the outer boundary to absorb outgoing waves [46].

the top plate, and the reflected and transmitted flexural waves are $w_r = s_r H_l^{(1)}(k\rho)e^{il\phi}$ on the top plate and $w_t = s_t H_l^{(1)}(k\rho)e^{il\phi}$ on the bottom plate outside the tunnel, where $H_l^{(1)}$ and $H_l^{(2)}$ are the lth-order Hankel function of the first and second kind. Then, the tunneling efficiency is expressed by $T = |s_t/s_{\text{in}}|^2$.$s_r$ and s_t can be extracted from the simulated total field pattern $w(r, \phi)$ (see Ref. [39]). Figure 3(b) shows that T against tunnel radius a stays near unity for $a > 14$ mm. For a smaller a, mode conversion into other membrane modes can happen with $T < 1$. We also note that the vortex tunneling is robust against a small shift of the focusing center [39].

We further experimentally demonstrate the tunneling effect through the elastic curved plate implementation. The curved elastic plate is fabricated using photopolymerization-based 3D printing technology. As shown in Fig. 4(a), two separated rectangular thin plates with size 280×180 mm^2 are linked by the tunnel with the same geometric parameters of Fig. 1(c). A Polytec PSV-400 laser scanning vibrometer is used to measure the out-of-plane displacement profile of the wormhole structure in our work [39]. We first consider a point source located at $P(X_1 = -80\text{ mm}, 0)$ on the top plate with wavelength $\lambda = 11.5$ mm. Figure 4(b) shows the measured displacement field distribution on the top plate ($z \geq 0$), with cylindrical wave front from the point source (the dashed circle indicates $\rho = b$). Part of this wave front (within ±28°) is captured by the wormhole and tunnels to the bottom plate.

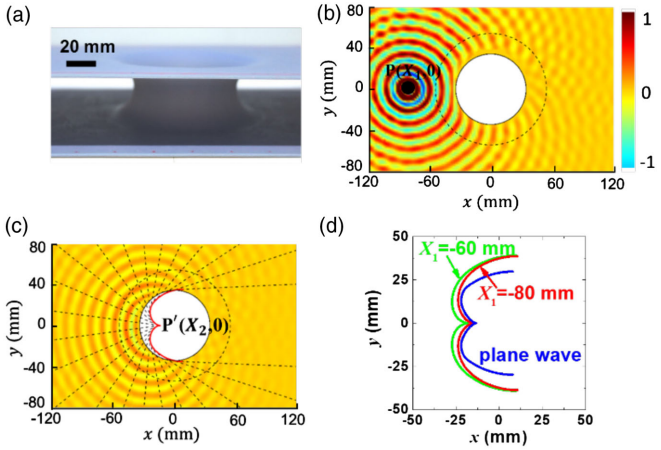

FIG. 4. Experimental observation of the wave propagation and virtual caustic of the wormhole. (a) The 3D printed sample: two separated thin plates (280×180 mm^2) linked by a tunnel with same dimension in Fig. 1(c) but with thickness $d_0 = 1.5$ mm. (b) Out-of-plane displacement field on the top plate. A point source is located at $P(X_1 = -80\ \text{mm}, 0)$. (c) The field pattern on the bottom plate and the virtual caustic (red line) with the same color bar in (b). (d) Virtual caustic lines for the point source located at $X_1 = -60$ mm (green), 80 mm (red), or an incidence plane wave (blue) coming along the positive x axis.

Equivalently, the wormhole blocks a part of the wave front of the area $a \le |\rho| \le b$ and leaves a shadow on the right. The tunneled out-of-plane displacement field on the bottom plate ($z \le 0$) is shown in Fig. 4(c). At first sight, it looks like the field comes from a virtual image of a point source. However, if we treat the system in the paraxial limit with the virtual image found by ray tracing at $(x, y) = (-14.7\ \text{mm}, 0)$, the measured field pattern does not fit well with the wave front from such a single point virtual image. In the case of the curved space here, the paraxial limit, e.g., on usual optical components, has limited usage. A more detailed analysis by constructing rays in the backward direction as perpendicular lines from the wave front shows that the rays come from an extended envelope instead of coming from a virtual image point. We call such an envelope a virtual caustic (defined in a similar sense as caustic in optics where light rays converge to form such an envelope). The virtual caustic is shown as the red curve in Fig. 4(c), while the black dashed lines are the rays to construct the caustic. The measured out-of-plane displacement field and the caustic coincide with those obtained by scalar wave simulation (TO based) and 3D flexural wave simulation [39].

The caustic line is robust against the location of the exciting point source, and it is actually the signature of the curved space of the wormhole. Two extreme cases for the point source located at $P(X_1 = -60\ \text{mm}, 0)$ on the top plate (near the surface of the tunnel) and an incident plane wave coming along the positive x direction are further studied [39]. For comparison, we plot the extracted virtual caustics for the three cases in Fig. 4(d). It demonstrates that the caustics have a similar location with the "tip" from near zero angle at around $P'(X_2 = -16\text{mm}, 0)$ and with a similar shape. In fact, the location of the tip $P'(X_2, 0)$ and the source location $P(X_1, 0)$ are related to each other by the following "lens" formula [39]:

$$\frac{1}{X_1} + \frac{1}{X_2} = -\int \frac{1}{\rho^2} |dr|. \tag{2}$$

Based on this formula, the location of the tip point is actually more sensitive to the geometric curvature of the wormhole [tunnel radius a affecting the rhs of Eq. (2)] and robust against source location X_1 as demonstrated through ray tracing in the Supplemental Material Fig. S10 [39]. Specifically, we have obtained an average value $X_2 = -9$, -16, -25 mm by varying X_1 from ray-tracing results for the case of $a = 2\lambda$, 3λ, 4λ, which matches well with results from Eq. (2) [39].

In conclusion, we have turned and visualized the embedding diagram of a wormhole in 3D Euclidean space into an implementation using an elastic curved plate using pure geometric curvature. We have investigated the scalar wave propagation in curved space around the analog wormhole theoretically by TO theory and experimentally by 3D printing the curved plate and measuring the out-of-plane displacement field for flexural waves propagating on it. The out-of-plane displacement of the 3D curved elastic plate approximately satisfies the same scalar wave equation as realization. The wave redirection, tunneling effects of the beam, and vortex wave around the analog wormhole have been investigated. Our investigations can lead us to mimic and study other cosmological objects based on pure geometric curvature. The geometric curvature approach can also be applied to other TO applications for waveguiding, lensing, sensing, and communication on curved surfaces in both acoustic and optical domains.

This work is supported by Research Grants Council of Hong Kong (Grant No. 16302218). T. C. and J. Z. acknowledge financial support from NSFC (Grants No. 51675402 and No. 51275377), the Major Projects of NSFC (Grants No. 41390450 and No. 41390454), and support from CSC. Y. L. acknowledges the Fellowship of Future Scientists from the CSC. Z. L. acknowledges the financial support by NSFC (Grants No. 61505114 and No. 11574216).

*Corresponding author.
jensenli@ust.hk
†These authors contributed equally to this work.

[1] J. B. Pendry, D. Schurig, and D. R. Smith, Science **312**, 1780 (2006).
[2] U. Leonhardt, Science **312**, 1777 (2006).
[3] D. Schurig, J. J. Mock, B. J. Justice, S. A. Cummer, J. B. Pendry, A. F. Starr, and D. R. Smith, Science **314**, 977 (2006).

[4] L. H. Gabrielli, J. Cardenas, C. B. Poitras, and M. Lipson, Nat. Photonics **3**, 461 (2009).
[5] T. Ergin, N. Stenger, P. Brenner, J. B. Pendry, and M. Wegener, Science **328**, 337 (2010).
[6] Y. Lai, J. Ng, H. Y. Chen, D. Z. Han, J. J. Xiao, Z. Q. Zhang, and C. T. Chan, Phys. Rev. Lett. **102**, 253902 (2009).
[7] C. Li, X. Meng, X. Liu, F. Li, G. Fang, H. Chen, and C. T. Chan, Phys. Rev. Lett. **105**, 233906 (2010).
[8] M. Rahm, D. Schurig, D. A. Roberts, S. A. Cummer, and J. B. Pendry, Photonics Nanostructures Fundam. Appl. **6**, 87 (2008).
[9] W. X. Jiang, T. J. Cui, Q. Cheng, J. Y. Chin, X. M. Yang, R. Liu, and D. R. Smith, Appl. Phys. Lett. **92**, 264101 (2008).
[10] U. Leonhardt, New J. Phys. **11**, 093040 (2009).
[11] N. Kundtz and D. R. Smith, Nat. Mater. **9**, 129 (2010).
[12] T. Zentgraf, Y. Liu, M. H. Mikkelsen, J. Valentine, and X. Zhang, Nat. Nanotechnol. **6**, 151 (2011).
[13] J. Li and J. B. Pendry, Phys. Rev. Lett. **101**, 203901 (2008).
[14] T. Tyc and U. Leonhardt, New J. Phys. **10**, 115038 (2008).
[15] R. C. Mitchell-Thomas, T. M. McManus, O. Quevedo-Teruel, S. A. R. Horsley, and Y. Hao, Phys. Rev. Lett. **111**, 213901 (2013).
[16] U. Leonhardt and T. G. Philbin, New J. Phys. **8**, 247 (2006).
[17] T. G. Philbin, C. Kuklewicz, S. Robertson, S. Hill, F. König, and U. Leonhardt, Science **319**, 1367 (2008).
[18] T. G. Mackay and A. Lakhtakia, Phys. Lett. A **374**, 2305 (2010).
[19] D. A. Genov, S. Zhang, and X. Zhang, Nat. Phys. **5**, 687 (2009).
[20] C. Sheng, H. Liu, Y. Wang, S. N. Zhu, and D. A. Genov, Nat. Photonics **7**, 902 (2013).
[21] I. I. Smolyaninov, Y. J. Hung, and E. Hwang, Phys. Lett. A **376**, 2575 (2012).
[22] G. Lefebvre, M. Dubois, R. Beauvais, Y. Achaoui, R. K. Ing, S. Guenneau, and P. Sebbah, Appl. Phys. Lett. **106**, 024101 (2015).
[23] M. W. McCall, A. Favaro, P. Kinsler, and A. Boardman, J. Opt. **13**, 024003 (2010).
[24] I. I. Smolyaninov and E. E. Narimanov, Phys. Rev. Lett. **105**, 067402 (2010).
[25] A. Greenleaf, Y. Kurylev, M. Lassas, and G. Uhlmann, Phys. Rev. Lett. **99**, 183901 (2007).
[26] M. D. Kruskal, Phys. Rev. **119**, 1743 (1960).
[27] M. S. Morris, K. S. Thorne, and U. Yurtsever, Phys. Rev. Lett. **61**, 1446 (1988).
[28] M. Kadic, G. Dupont, S. Enoch, and S. Guenneau, Phys. Rev. A **90**, 043812 (2014).
[29] V. H. Schultheiss, S. Batz, A. Szameit, F. Dreisow, S. Nolte, A. Tünnermann, S. Longhi, and U. Peschel, Phys. Rev. Lett. **105**, 143901 (2010).
[30] A. A. Evans and A. J. Levine, Phys. Rev. Lett. **111**, 038101 (2013).
[31] R. Bekenstein, Y. Kabessa, Y. Sharabi, O. Tal, N. Engheta, G. Eisenstein, A. J. Agranat, and M. Segev, Nat. Photonics **11**, 664 (2017).
[32] A. Aubry, D. Y. Lei, S. A. Maier, and J. B. Pendry, Phys. Rev. Lett. **105**, 233901 (2010).
[33] V. Ginis, P. Tassin, C. M. Soukoulis, and I. Veretennicoff, Phys. Rev. Lett. **110**, 057401 (2013).
[34] D. Smirnova, S. H. Mousavi, Z. Wang, Y. S. Kivshar, and A. B. Khanikaev, ACS Photonics **3**, 875 (2016).
[35] J. Bae, H. Cho, K. Song, H. Lee, and H. J. Yoo, IEEE Trans. Microwave Theory Tech. **60**, 582 (2012).
[36] W. Xuan, M. He, N. Meng, X. He, W. Wang, J. Chen, T. Shi, T. Hasan, Z. Xu, Y. Xu, and J. K. Luo, Sci. Rep. **4**, 7206 (2014).
[37] F. Guo, Z. Mao, Y. Chen, Z. Xie, J. P. Lata, P. Li, L. Ren, J. Liu, J. Yang, M. Dao, S. Suresh, and T. J. Huang, Proc. Natl. Acad. Sci. U.S.A. **113**, 1522 (2016).
[38] M. S. Morris and K. S. Thorne, Am. J. Phys. **56**, 395 (1988).
[39] See Supplemental Material at http://link.aps.org/supplemental/10.1103/PhysRevLett.121.234301 for further theoretical and experimental details.
[40] E. F. I. Niordson, *Shell Theory* (North-Holland, Amsterdam, 1985).
[41] Y. H. Pao and C. C. Mow, *Diffraction of Elastic Waves and Dynamic Stress Concentrations* (Crane, Russak, New York, 1973).
[42] F. M. Li, C. Hu, and W. H. Huang, J. Sound Vib. **259**, 1209 (2003).
[43] M. Farhat, S. Guenneau, and S. Enoch, Phys. Rev. Lett. **103**, 024301 (2009).
[44] N. Stenger, M. Wilhelm, and M. Wegener, Phys. Rev. Lett. **108**, 014301 (2012).
[45] A. Diatta, A. Younes, and S. Guenneau, arXiv:1802.01488.
[46] A. Diatta, M. Kadic, M. Wegener, and S. Guenneau, Phys. Rev. B **94**, 100105 (2016).